PROCEEDINGS, 51st Workshop on Geothermal Reservoir Engineering
Stanford University, Stanford, California, February 9-11, 2026
SGP-TR-230

Effects of Particle Breakage on the Hydro-mechanical Behavior of Proppant Packs

Ayat Alasadi and Shahrzad Roshankhah

Civil & Environmental Engineering, The University of Utah, Salt Lake City, UT

Shahrzad.Roshankhah@utah.edu

Keywords: Proppant breakage, Discrete element method (DEM), Fragment replacement method (FRM), Permeability evolution, Micro–macro behavior, Enhanced geothermal systems (EGS)

ABSTRACT

Proppant packs are essential for maintaining fracture conductivity in enhanced geothermal systems (EGS). However, under the EGS high closure stresses and elevated temperatures, the long-term hydraulic performance is strongly affected by particle crushing, resulting in permeability reduction. This study presents a three-dimensional discrete element modeling investigation of proppant pack settlement, particle breakage, and permeability evolution under stress conditions representative of the Utah FORGE geothermal site. Simulations are performed using Particle Flow Code in three dimensions (PFC3D), in which particle fracture is captured through a Fragment Replacement Method (FRM). Breakage is triggered when a stress derived from the maximum contact force exceeds a size-dependent characteristic strength, calibrated using single-particle diametral compression test data. Loading is applied incrementally under oedometric conditions, with breakage events followed by mechanical re-equilibration to mitigate numerical artifacts. Pack-scale void ratio evolution is quantified from volumetric changes associated with particle rearrangement and fragmentation, while permeability evolution is estimated using the Kozeny–Carman relationship. Results show that allowing particle breakage leads to a more compliant macroscopic response, progressive broadening of the particle size distribution, and a sustained reduction in permeability driven by the generation of fines and reorganization of the contact network. Breakage is found to be distributed throughout the pack and governed primarily by internal force-chain evolution rather than boundary effects. These findings highlight the mechanical response to proppant crushing and provide a quantitative framework for evaluating trade-offs between particle size and strength when selecting proppants to maintain fracture conductivity in EGS and unconventional energy reservoirs.

1. INTRODUCTION

Proppant particle size distribution (PSD) and shape play a central role in governing pack formation within hydraulic fractures and the hydromechanical response of proppant packs under loading (Zhou et al., 2016; Balushi et al., 2024; Ali et al., 2024; Adesina et al., 2024). Under high closure stresses, however, proppant particles can fracture into smaller fragments, leading to a significant reduction in permeability through blockage of flow paths (Rivers et al., 2012).

Particle breakage has been investigated using laboratory experiments and discrete element method (DEM) simulations. Diametral compression tests on individual particles reveal multiple fracture modes controlled by particle size, internal flaw distribution, and loading rate. Despite these variations, diametral splitting is most commonly observed as the dominant fracture mechanism (Zheng and Tannant, 2018a; Zhou et al., 2020). DEM simulations have reproduced realistic particle-size-dependent mechanisms of crack initiation and crushing strength, and fragment-size distributions observed in laboratory tests (Meng et al., 2017). Combined laboratory experiments and DEM simulations on carbonate sand particles identified distinct loading stages leading to either tensile splitting or explosive fragmentation, with fracture behavior strongly controlled by particle morphology and intra-particle porosity (Dong et al., 2024). Particles with lower sphericity consistently exhibit more severe fragmentation and higher degrees of fractal breakage, whereas highly spherical particles sustain higher crushing loads and promote more uniform stress transmission (Cai et al., 2024). Particle geometry and contact orientation strongly govern fracture evolution, including splitting, corner breakage, and progressive fragmentation. Angular particles develop more complex fracture patterns than spherical particles due to heterogeneous contact forces and stress concentrations (Wang et al., 2017).

The behavior of particle fracture within a granular pack is governed by the redistribution of forces through evolving contact networks, in which coordination number, force-chain structure, and confinement control failure mechanisms (McDowell and de Bono, 2013; Zheng and Tannant, 2018b; Cil and Alshibli, 2014). Under one-dimensional compression (i.e., oedometer tests), fracture occurs when force chains impose stresses that exceed particle strength, with breakage typically initiating in particles located closest to the loading platen (Shi et al., 2016). Large particles often fail first because they generally exhibit lower coordination numbers, meaning they engage with fewer neighboring contacts and therefore carry higher forces per contact (Cil and McDowell, 2007). Also, large particles may have a greater number of defects, making them more susceptible to breakage. In contrast, smaller particles tend to have higher coordination numbers, allowing the applied load to be distributed over more contacts and reducing contact forces (Wiacek and Molenda, 2014). In situ synchrotron micro-tomography observations further show that particle fracture and generation of fines progressively alter contact configurations and load redistribution within the pack (Cil and Alshibli, 2014; Xu, 2018).

Two main DEM-based approaches are commonly used to simulate particle breakage: the bonded particle method (BPM) and the fragment replacement method (FRM). In BPM, individual particles are represented as agglomerates of bonded sub-particles, and breakage occurs through instantaneous bond failure once local stresses exceed the bond strength, allowing for the explicit simulation of crack initiation

and propagation within particles (Potyondy and Cundall, 2004; McDowell and Harireche, 2002; Cheng et al., 2003). While BPM can capture particle size and shape effects and fracture mechanisms with high fidelity, it is computationally demanding and is therefore primarily suited for single-particle studies or small assemblies. In contrast, FRM models particle breakage by deleting a parent particle and replacing it with a predefined set of smaller, unbonded spherical fragments once a stress- or force-based breakage criterion is satisfied (Åström and Herrmann, 1998; Tsoungui et al., 1999; McDowell and de Bono, 2013). FRM enables efficient simulation of particle breakage with lower computational cost at the specimen and engineering scales, making it well-suited for pack-scale analyses. However, the method requires careful selection of breakage criteria and fragment number, as these choices significantly influence mass conservation, local stress redistribution, and numerical stability (Ciantia et al., 2015; Wu et al., 2022).

Existing studies primarily focus on macroscopic stress–strain behavior, force-chain evolution, or changes in particle size distribution, while relatively limited attention has been given to how breakage-induced microstructural reorganization governs the evolution of permeability. This study addresses this gap by investigating how particle breakage influences the pack's permeability evolution, and how breakage is distributed throughout a proppant pack under oedometric loading. Particle breakage is simulated using the fragment replacement method (FRM) implemented in PFC3D (Itasca, 2025), in which breakage is triggered when the stress derived from the maximum contact force exceeds the particle's size-dependent tensile strength. Upon failure, each parent particle is replaced by child particles with equivalent total volume, ensuring mass conservation. The permeability evolution associated with progressive particle breakage, including original particles, broken fragments, and packing rearrangement, is quantified using the Kozeny–Carman relationship (Kozeny, 1927). Through this framework, the study provides insight into the mechanisms controlling permeability degradation in proppant packs under loading conditions representative of enhanced geothermal systems (EGS).

2. SINGLE PARTICLE BREAKAGE

Single-particle diametral compression tests provide key mechanical properties of proppant particles, including crushing strength, elastic stiffness, fracture mode, and the statistical variability of strength (Bandara et al., 2020). In this study, the individual particle-diameter test data reported by Anaya et al. (2022) are used as a reference to calibrate particle breakage parameters under the adopted breakage scheme. A total of 50 individual ceramic proppant particles were subjected to quasi-static diametral compression until failure (i.e., particle breakage), as illustrated in Figure 1. The tested ceramic proppant has an average initial particle diameter d_0 = 0.6 mm, roundness and sphericity of 0.8 and 0.9, respectively, Young's modulus E = 56 GPa, and particle density ρ_p = 1.56 g/cm.

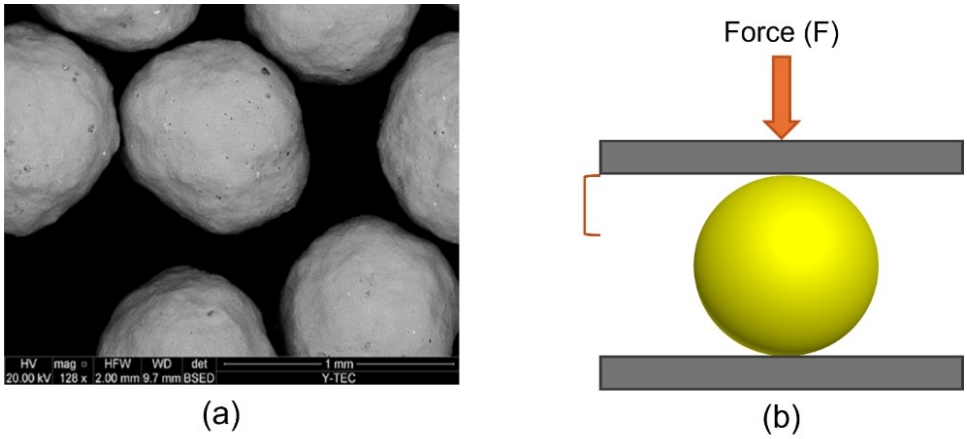

Figure 1: Microstructural characterization of the studied proppant particles: (a) An SEM image of the carbo ceramic proppant particles (Anaya et al. 2022), and (b) a 2D schematic view of the diametral compression test.

For tested particles, the peak force at failure, F_{peak}, was extracted from the force–displacement response and used to calculate the average characteristic particle strength, $\sigma_0 = F_{peak}/d_0^2$ = 170 MPa. The size dependence of particle strength, whereby smaller particles exhibit higher apparent strength due to a reduced probability of critical internal flaws. This size effect is commonly described using Weibull theory (Weibull, 1951), in which the crushing strength of a particle of diameter d is given by

$$\sigma_s(d) = \sigma_0\left(\frac{d}{d_0}\right)^{-3/m}, \quad (1)$$

where d_0 = 0.6 mm is the reference (characteristic) diameter, σ_0 is the characteristic strength associated with d_0, and m is the Weibull modulus. Based on a Weibull statistical analysis of the experimental results, Anaya et al. reported a Weibull modulus m = 4.2, indicating a brittle fracture response with moderate scatter. Under this formulation, $\sigma_s(d)$ represents the crushing strength of particles of diameter d corresponding to a survival probability P_s = 37%. As σ approaches σ_0, the survival probability decreases sharply as contact stresses exceed the critical strength of pre-existing internal flaws, triggering particle failure (McDowell and Bolton, 1998). Scanning electron microscopy (SEM) observations and force–displacement curves reported by Anaya et al. (2022) indicate a brittle fracture response, with particles exhibiting nonlinear behavior up to a well-defined peak load followed by sudden failure, as shown in Figure 2.

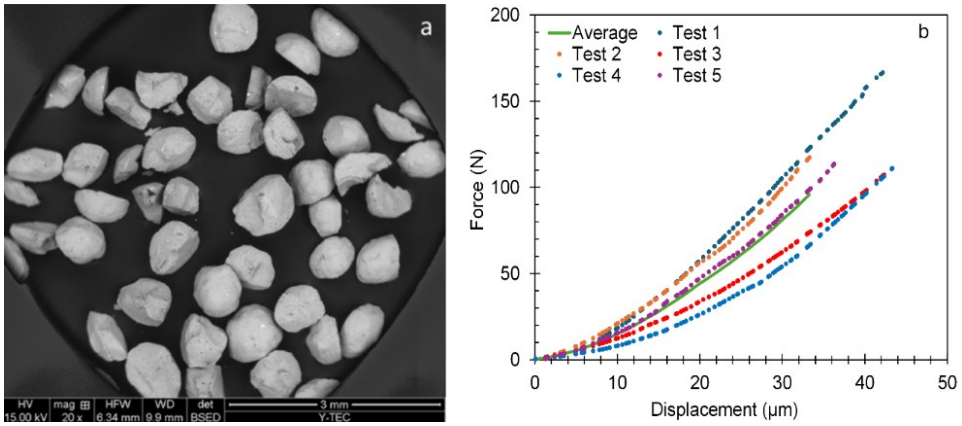

Figure 2: Diametral test results on ceramic proppant: (a) SEM images after mechanical testing, and (b) force versus displacement curves (Anaya et al., 2022).

3. NUMERICAL MODELING

3.1 Oedometer Test Model

To investigate the behavior of the proppant pack, a cylindrical specimen is modeled under oedometric loading conditions using PFC3D (Itasca, 2025). The oedometer simulation consists of two stages: (1) a particle-settlement phase with a cylindrical rigid cell and (2) a one-dimensional compression phase using a disk-shaped rigid platen set to move downward at a constant rate of 0.1 m/s to apply axial stress σ_a, as shown in Figure 3. A damping coefficient α of 0.7 is used to dissipate kinetic energy and suppress inertial oscillations, thereby maintaining a quasi-static response during particle rearrangement and breakage.

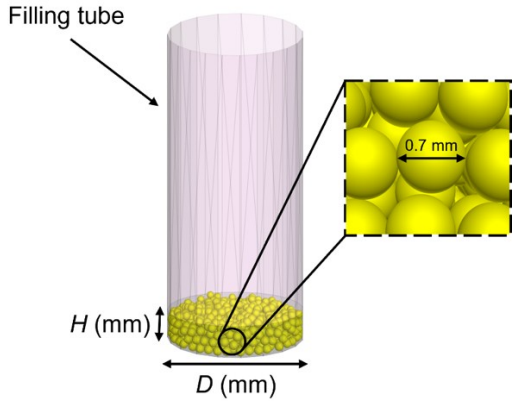

Figure 3: DEM oedometer model cell setup in PFC3D.

The physical proppant pack is expected to exhibit a nonlinear elastic response (Alasadi et al., 2025) similar to that observed at the single-particle scale prior to brittle failure. Accordingly, the Hertzian contact model is employed to describe particle–particle interactions, while a linear contact model is used for particle–wall contacts. A detailed mathematical formulation of the numerical model is provided elsewhere (Alasadi et al., 2025; Potyondy, 2025). The Hertzian contact model parameters include the particle Young's modulus E_p, Poisson's ratio ν_p, particle density ρ_p, and the inter-particle friction coefficient μ_p. The linear contact model parameters include the normal wall stiffness k_{nw}, the wall shear stiffness k_{sw}, and the wall friction coefficient μ_w (Potyondy, 2025).

A particulate pack is generated within an oedometer cell with a diameter D = 10 mm and a height H = 2 mm. This is a scaled-down model of the laboratory counterpart, with D = 63 mm and H = 17 mm, conducted with resin-coated low-density proppant (LDC) (see Figure 4(a)) and loaded to σ_a. = 35 MPa. These dimensions are selected to conform to the ASTM D2435 recommended height-to-diameter (H/D) ratios for oedometer testing, thereby minimizing boundary effects (ASTM, 2025). The relatively small specimen height implies that, at the onset of loading, short force chains develop between the top platen and bottom wall, allowing the simulation to reach high stress levels within a feasible computational time (Ciantia et al., 2015). At the same time, the chosen diameter is sufficiently large to permit the development of multiple force chains within the pack, ensuring a representative internal stress network (Läzel et al., 2000; Marketos and Bolton, 2009). The selected geometry, therefore, represents a compromise between one-to-one similarity to physical and computational efficiency.

In this study, two dense, randomly generated packs of 455 spherical proppant particles with d_0 = 0.7 mm are created and subjected to oedometric loading under quasi-static conditions. In one pack, particles are assumed to remain intact throughout loading (unbreakable pack), while in the other, particle breakage is allowed and modeled using the approach described above (breakable pack). The DEM model is calibrated by first ensuring that the contact model reproduces the specimen's initial elastic response. Particle breakage parameters,

including the reference particle strength $\sigma_0(d_0)$ and the Weibull modulus m, are then fine-tuned to match the experimentally observed stress–strain behavior and breakage evolution. The calibrated parameters are summarized in Table 1.

Table 1: Microscopic parameters used in the DEM model.

Parameter	Value
Particle size, d_0 (mm)	0.7
Particle density, ρ_p (g/cc)	1.2
Initial void ratio, e_0	0.9
Hertzian Contact Model	
Young's modulus, E_p (GPa)	11
Poisson's ratio, ν_p	0.2
Interparticle friction coefficient, μ_p	0.5
Linear Contact Model	
Wall normal stiffness, k_{nw} (GPa)	1
Wall shear stiffness, k_{sw} (GPa)	1
Wall friction coefficient, μ_w	0.0
Local damping coefficient, α	0.7
Fragment Replacement Method	
Weibull modulus, m	3
Characteristic particle strength, $\sigma_0(d_0)$ (MPa)	90

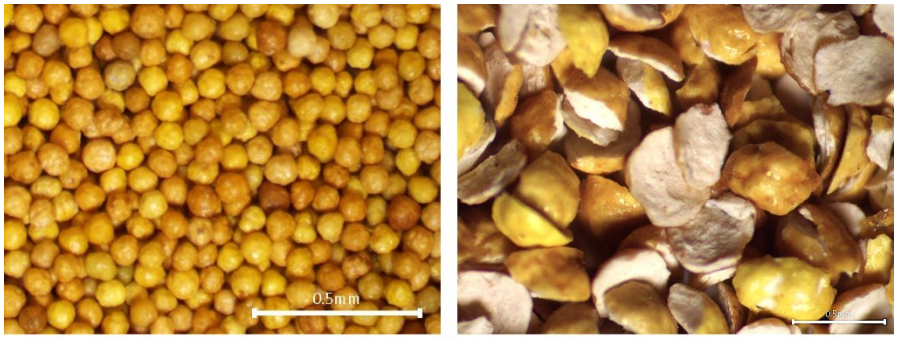

(a) (b)

Figure 4: (a) Resin-coated low-density ceramic proppant particles before loading, and (b) broken particles after 35 MPa axial loading.

3.2 Particle Breakage Modeling

In PFC, particles are treated as rigid bodies with finite mass that can translate and rotate but cannot fracture intrinsically (Zhang et al., 2024). The deformations are concentrated at the soft contacts with properties listed in Table 1. Particle breakage is therefore incorporated using the fragment replacement method (FRM) framework (McDowell and Bolton, 1998). When adopting the FRM approach, two key aspects must be specified: (1) the breakage criterion and (2) the number of fragments generated during each breakage event. Several breakage criteria have been proposed in the FRM literature to govern particle failure. Among these, the octahedral shear stress, q, and the stress induced by the maximum normal contact force, σ_{max}, have been shown to successfully reproduce the macroscopic behavior of crushable granular materials (de Bono and McDowell, 2016a). In this study, the σ_{max} criterion is adopted and defined as

$$\sigma_{max} = \frac{F^c_{max}}{d^2}, \tag{2}$$

where d (mm) is the particle diameter and F^c_{max} (N) is the maximum normal contact force acting on the particle. Particle breakage is triggered when $\sigma_{F_{\max}} > \sigma_s(d)$, where $\sigma_s(d)$ is the size-dependent particle strength.

The number of child particles generated during breakage is selected to ensure mass conservation within the numerical simulation. The underlying assumption is that any mass loss associated with unresolved fines corresponds to particles smaller than whose influence on the macroscopic mechanical response is negligible (Radjai et al., 1996). Previous studies have shown that varying the number of fragments produced per breakage event has little influence on the normal compression response or the evolving particle size distribution, provided that mass conservation is maintained and the particle strength–size relationship remains unchanged, as the macroscopic behavior is controlled primarily by the size-dependent hardening law rather than the specific fragmentation geometry (McDowell and de Bono, 2013).

In this study, when the breakage criterion is satisfied, the parent particle is replaced by two non-overlapping child particles whose combined volume equals that of the original particle. Given the particles' incompressibility, this ensures mass conservation. This

replacement scheme provides a computationally efficient and mechanically representative approach for modeling particle breakage at the pack scale, as illustrated in Figure 5(a). During loading, the breakage criterion is evaluated by looping over all particles in the pack, and particles for which the breakage criterion is met are replaced by child particles with properties identical to those of the parent particle (de Bono and McDowell, 2016b). Figure 5(b) illustrates the breakage scheme adopted in this study, in which the specimen is loaded incrementally, and the breakage criterion is evaluated at regular intervals during deformation. When the maximum stress proxy acting on a particle exceeds its size-dependent characteristic strength, loading is temporarily halted, and the parent particle is replaced by smaller child particles.

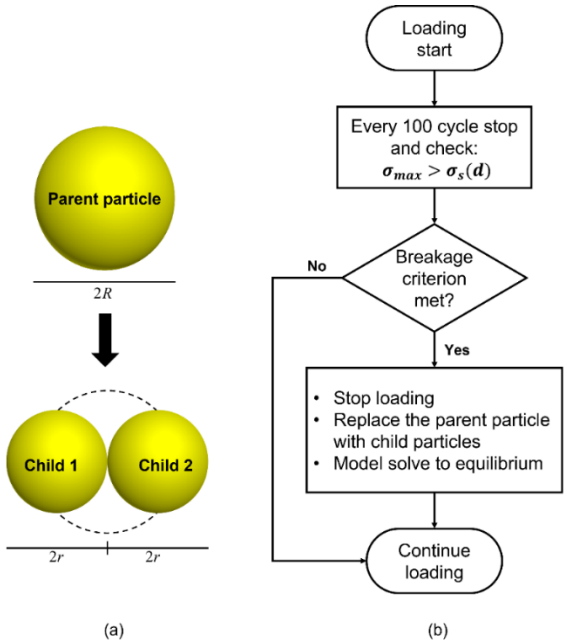

Figure 5: Fragment replacement method (FRM) breakage scheme used in this study: (a) Replacement of a parent particle by two child particles upon satisfaction of the breakage criterion, and (b) Schematic of the loading–breakage procedure.

The system is then allowed to reach mechanical equilibrium before loading is resumed. This stop–replace–equilibrate–resume procedure is adopted to reduce numerical amplification of force and stress spikes commonly associated with particle replacement in FRM-based simulations. Although transient stress spikes are physically expected during particle crushing in laboratory experiments, their magnitude can be artificially amplified in DEM simulations due to the abrupt release of stored elastic energy following the deletion of a stressed parent particle and the insertion of child particles (Wu et al., 2022). By temporarily halting loading and allowing the system to re-equilibrate before deformation is resumed, these transient numerical effects are attenuated, ensuring that the reported axial stress corresponds to a mechanically stable configuration after each breakage event. The remaining spikes are removed through post-processing of the output data.

4. RESULTS AND DISCUSSION

4.1 Macroscopic Response

Figure 6(a) compares the macroscopic stress–strain responses of the model packs consisting of breakable and unbreakable particles with the experimental results. After an initial stage dominated by particle rearrangement, the model pack with unbreakable particles deviates from the experimental response, starting at 0.08 strain and continuing to strain harden, suggesting that particle breakage must have softened the macroscopic mechanical behavior of the proppant pack in the laboratory test. The response of the model pack with breakable particles is softer than that of the pack with unbreakable particles, and it starts showing breakage around the same point where the unbreakable particles continue to strain hardening. However, the calibrated model of breakable particles shows more compliant behavior than the laboratory results beyond 0.12 axial strain. This softening is likely due to the amount of particle breakage developed in the pack and the use of two child particles per breakage event. The spikes in the breakable pack indicate unbalanced forces due to breakage events. This breakage results in a broader particle size distribution and an increase in the total particle count to 834, indicating that approximately 33% of the original particles experienced breakage compared to less than 5% measured in the laboratory by the end of loading at 35 MPa axial stress. These observations indicate that the proppant candidate used in this study does not exhibit significant degradation at 35 MPa. In the unbreakable pack, the particle size distribution remains constant throughout loading, as particles are preserved and no fragmentation occurs. Figure 6(b) presents the particle size distributions (PSDs) of the two packs at the end of loading compared to those in the laboratory.

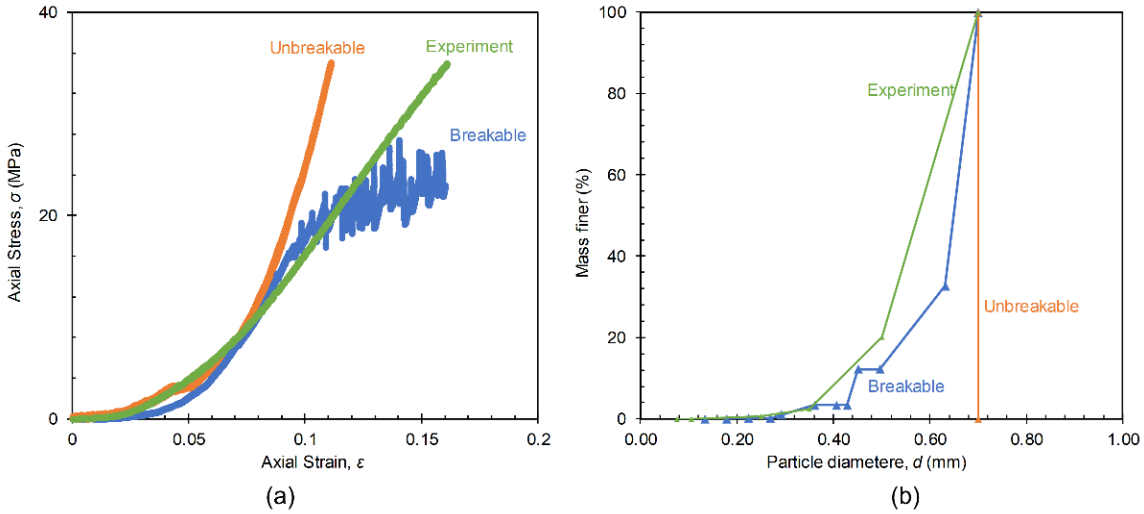

Figure 6: Macroscopic response of proppant pack models assuming breakable and unbreakable particles compared to that in the laboratory test: (a) axial stress-strain curves, and (b) particle size distribution (PSD) before and after the laboratory and numerical oedometer tests.

4.2 Permeability Evolution

Permeability, K (m^2), reflects the connectivity of void spaces within the particle pack and is strongly influenced by particle shape (Banala et al., 2019) and size distribution (Tang et al., 2023). The permeability evolution of packs with spherical particles can be approximated using the Kozeny–Carman relationship (Kozeny, 1927):

$$K = \frac{1}{S_0^2 (C_{C-K})} \frac{e^3}{1+e} \quad , \tag{4}$$

where C_{C-K} is the dimensionless Kozeny–Carman empirical coefficient, assumed to be 5 for uniform spherical particles. S_0(m^{-1}) is the volumetric specific surface of the particles, defined as the particle surface area per unit volume, and e is th e void ratio of the particle assembly (Rehman et al., 2024; Mauran et al., 2001).

Figure 7 presents the evolution of proppant pack permeability for model packs of unbreakable and breakable particles. All packs start with the same initial permeability of e_0 = 0.9. At axial stress = 30 MPa, where the breakable particle pack shows the last stress reading, the unbreakable pack has higher permeability, retaining about 51% of its initial permeability as the particles remain intact throughout loading, and the reduction is associated with particle rearrangement only. The breakable pack retains 40% of its permeability, similar to the permeability calculated in the laboratory. This reduction is driven by particle breakage and subsequent rearrangement, causing disruption of inter-particle void connectivity, consistent with the experimental findings but with a slightly different trend (Wang et al., 2019).

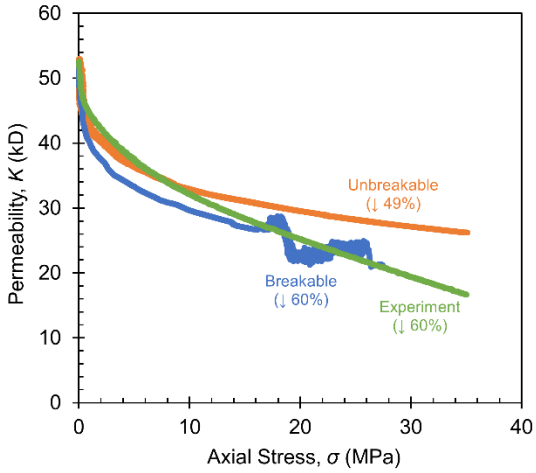

Figure 7: Proppant permeability evolution under oedometric loading up to 35 MPa and 70 MPa.

4.3 Particle Breakage Evolution

Figure 8 shows the particle breakage and the contact force distribution in the DEM models. Figure 8(a) shows the pack's initial configuration, in which the pack consists of intact parent particles settled under gravity to reach the specified void ratio, where the contact

forces are weak and uniform. Figure 8(b) shows the contact force distribution of the model pack of unbreakable particles at 35 MPa. The contact forces increase in magnitude and are more evenly distributed across the pack and aligned along the loading direction. Therefore, the coordination number, *CN*, increases by around 60%, as shown in Figure 9(a).

Particle breakages appear to initiate closer to the top loading platen and propagate toward the bottom base, where the contact force is highest. The breakage starts randomly across the pack and localizes where it starts, as shown in Figure 8(c). This behavior indicates that once breakage begins in a local area, the packing structure and contact forces are redistributed, leading to an increase in the load concentration within that local zone (Cil and Alshibli, 2014). However, as the axial loading increases, breakage appears to transition from being localized to a more randomly distributed across the pack at the end of loading. The peak forces are also reduced because breakage tends to disrupt highly stressed force chains and promote stress redistribution by generating additional contacts and fragments, thereby limiting the growth of extreme contact forces, particularly at higher strain levels, as shown in Figure 8(d).

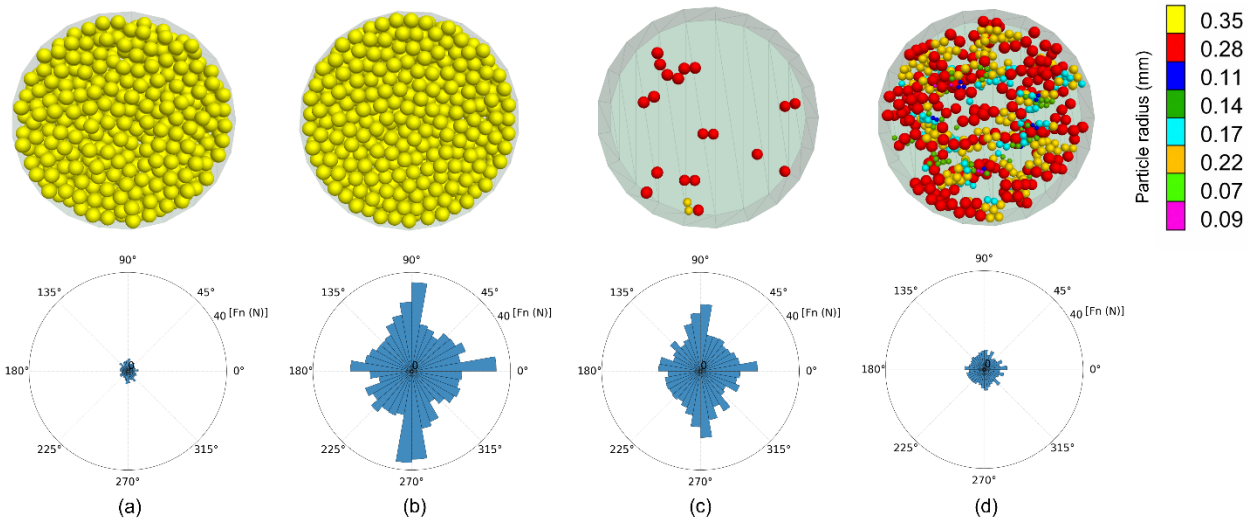

Figure 8: Particle breakage and contact force distribution in the proppant pack: (a) before loading, (b) unbreakable pack at 35 MPa, (c) breakable pack at the beginning of breakage, and (d) breakable pack at 35 MPa.

Figure 9(a) shows the evolution of coordination number (*CN*) with axial strain for the breakable and unbreakable packs. In both cases, *CN* increases similarly until breakage begins, due to particle rearrangement and pack densification. As loading continues, the *CN* of the breakable particles pack increases only modestly after the onset of particle breakage, with an overall increase of approximately 5%. This limited increase in *CN* is probably due to the relatively small increase in particle count (379 additional particles), as shown in Figure 9(b). This modest increase may be insufficient to significantly change the global *CN*.

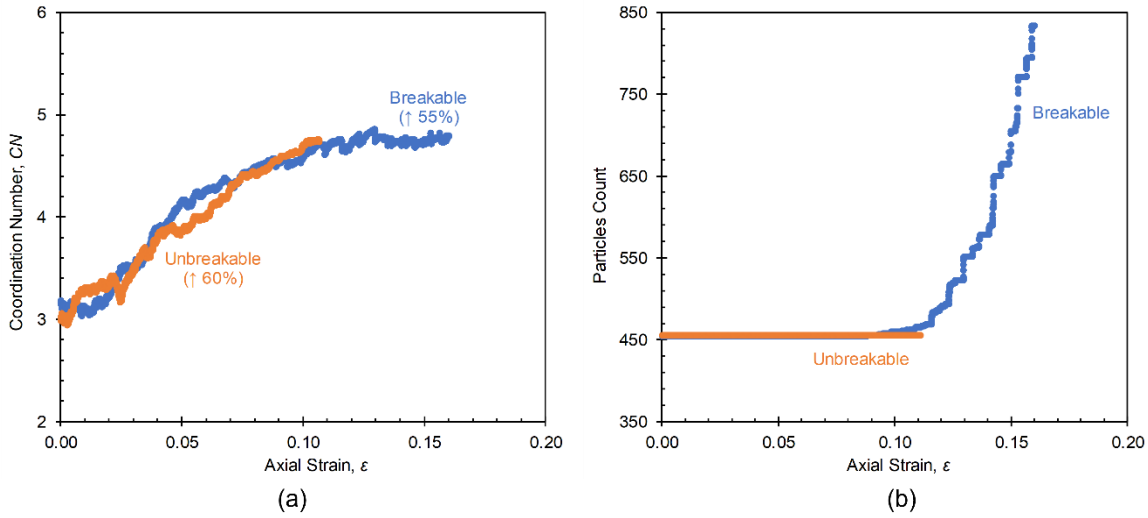

Figure 9: Strain-dependent evolution of microscale characteristics of model packs consisting of unbreakable and breakable particles under oedometric loading: (a) coordination number versus axial strain, and (b) particle count versus axial strain.

5. CONCLUSIONS

This study investigates the role of particle breakage in the mechanical and hydraulic response of proppant packs under oedometric loading conditions. A three-dimensional DEM framework incorporating a fragment replacement method (FRM) is developed and calibrated using single-particle diametral compression and oedometer data for ceramic proppants. The main conclusions are summarized as follows:

The adopted force-based breakage criterion reproduces a macroscopic mechanical response closer to the laboratory results than with unbreakable particles. Replacing each parent particle with two fragments provides an effective balance between physical resolution and computational efficiency, although a larger number of fragments may be used to improve the macroscopic match at an additional computational cost.

Particle breakage initiates in highly stressed regions closer to the loading platen and progressively propagates to the surrounding regions and intensifies with increasing applied stress. This evolution disrupts dominant force chains, increases coordination number via fragment generation, and redistributes stress, resulting in a more compliant macroscopic response and pronounced microstructural reorganization of the proppant pack. Particle breakage strongly governs permeability evolution. At modest fragment generation, a substantial permeability reduction is still observed. As axial loading increases, continued breakage and fabric reorganization drive a continuous loss of permeability, demonstrating that permeability reduction is primarily controlled by breakage-induced microstructural changes rather than by compaction alone.

This work demonstrates that accounting for particle breakage is essential for predicting the coupled mechanical and hydraulic response of proppant packs under high stress. Future model developments should focus on refining breakage representation by investigating the effect of fragment numbers and incorporating EGS-relevant temperature effects to improve proppant selection.

ACKNOWLEDGMENT

This project was sponsored by the US Department of Energy's National Energy Technology Laboratory and Geothermal Technology Office through Utah FORGE 2022 opportunity.

REFERENCES

ASTM International: Standard Test Methods for One-Dimensional Consolidation Properties of Soils Using Incremental Loading, ASTM D2435/D2435M-25, ASTM International, West Conshohocken, PA (2025).

Adesina, P., O'Sullivan, C., and Wang, T.: DEM study on the effect of particle shape on the shear behaviour of granular materials, Computational Particle Mechanics, 11(1), (2024), 447–466.

Alasadi, A., Ghassemi, A., Potyondy, D., and Roshankhah, S.: DEM-based analysis to reveal the effects of particle size distribution on deformational behavior of particulate packs (2025).

Ali, U., Kikumoto, M., and Ciantia, M.: Impact of particle elongation on the behavior of round and angular granular media: Consequences of particle rotation and force chain development, Computers and Geotechnics, 165, (2024), 105858.

Anaya, R., Martínez, J.M., Hernández, M.F., Herrera, M.S., and Rendtorff, N.M.: Individual diametral compression behavior of a ceramic proppant, Ceramics International, 48(21), (2022), 32357–32365.

Åström, J.A., and Herrmann, H.J.: Fragmentation of grains in a two-dimensional packing, European Physical Journal B, 5(3), (1998), 551–554.

Balushi, R.A., Ge, S., Fredrich, J., and Huang, H.: DEM–LBM modeling of shape effect on proppant transport and fracture permeability under geothermal conditions, Geothermics, 110, (2024), 102867.

Banala, A., Ma, H., and Kumar, A.: Influence of particulate geometry on permeability of porous materials, Powder Technology, 345, (2019), 704–716.

Bandara, K.M.A.S., Ranjith, P.G., and Rathnaweera, T.D.: Extensive analysis of single ceramic proppant fracture mechanism and the influence of realistic extreme reservoir conditions on proppant mechanical performance, Journal of Petroleum Science and Engineering, 195, (2020), 107586.

Bourret, R., Raphaël, E., and de Gennes, P.G.: Propagation of a pressure step in a granular material: The role of wall friction, Physical Review E, 55, (1997), 5759–5773.

Cai, P., Mao, X., Wu, Q., and Wang, Y.: Quantifying the influence of single particle shape on crushing characteristics of recycled aggregates: Experimental and numerical insights, Construction and Building Materials, 439, (2024), 137363.

Cheng, Y.P., Nakata, Y., and Bolton, M.D.: Discrete element simulation of crushable soil, Géotechnique, 53(7), (2003), 633–641.

Ciantia, M.O., Arroyo, M., Calvetti, F., and Gens, A.: An approach to enhance efficiency of DEM modelling of soils with crushable grains, Géotechnique, 65(2), (2015), 91–110.

Cil, M.B., and Alshibli, K.A.: 3D evolution of sand fracture under 1D compression, Géotechnique, 64(5), (2014), 351–364.

de Bono, J.P., and McDowell, G.R.: Particle breakage criteria in discrete-element modelling, Géotechnique, 66(12), (2016a), 1014–1027.

de Bono, J.P., and McDowell, G.R.: The fractal micromechanics of normal compression, Computers and Geotechnics, 78, (2016b), 11–24.

Dong, Z.-L., Cheng, Y.P., Tong, C.-X., Liu, H., Zhang, S., and Sheng, D.: DEM modeling of particle crushing of single carbonate sand using the improved bonded particle model, Powder Technology, 445, (2024), 120121.

Itasca Consulting Group, Inc.: PFC3D – Particle Flow Code in 3 Dimensions, Version 9.0 User's Manual, Minneapolis, MN (2025).

Kozeny, J.: Über kapillare Leitung des Wassers im Boden, Sitzungsberichte der Akademie der Wissenschaften, Mathematisch-Naturwissenschaftliche Klasse, 136(2a), (1927), 271–306.

Lätzel, M., Luding, S., and Herrmann, H.J.: Macroscopic material properties from quasi-static, microscopic simulations of a two-dimensional shear cell, Granular Matter, 2, (2000), 123–135.

Lim, W.L., and McDowell, G.R.: The importance of coordination number in using agglomerates to simulate crushable particles in the discrete element method, Géotechnique, 57(8), (2007), 701–705.

Lobo-Guerrero, S., and Vallejo, L.E.: Influence of pile shape and pile interaction on the crushable behavior of granular materials around driven piles: DEM analyses, Granular Matter, 9, (2007), 241–250.

Marketos, G., and Bolton, M.D.: Compaction bands simulated in discrete element models, Journal of Structural Geology, 31(5), (2009), 479–490.

McDowell, G.R., and Bolton, M.D.: On the micromechanics of crushable aggregates, Géotechnique, 48(5), (1998), 667–679.

McDowell, G.R., and de Bono, J.P.: On the micromechanics of one-dimensional normal compression, Géotechnique, 63(11), (2013), 895–908.

McDowell, G.R., and Harireche, O.: Discrete element modelling of yielding and normal compression of sand, Géotechnique, 52(4), (2002), 299–304.

Meng, Y., Cheng, Y., and Zhou, W.: DEM simulation of single particle crushing and extension to coarse particle strength characterization, Granular Matter, 19(4), (2017), 85.

Potyondy, D.: Material modeling support for PFC (Itspkg9.2), Report No. Itasca Consulting Group, Inc., Minneapolis, MN (2025).

Potyondy, D.O., and Cundall, P.A.: A bonded-particle model for rock, International Journal of Rock Mechanics and Mining Sciences, 41(8), (2004), 1329–1364.

Radjai, F., Jean, M., Moreau, J.-J., and Roux, S.: Force distributions in dense two-dimensional granular systems, Physical Review Letters, 77(2), (1996), 274–277.

Rivers, M., Zhu, D., and Hill, A.D.: Proppant fracture conductivity with high proppant loading and high closure stress, SPE Hydraulic Fracturing Technology Conference, The Woodlands, TX, USA (2012).

Shi, D., Zheng, L., Xue, J., and Sun, J.: DEM modeling of particle breakage in silica sands under one-dimensional compression, Acta Mechanica Solida Sinica, 29(1), (2016), 78–94.

Tang, Y., Wei, H., Chen, Y. et al. Modeling of permeability for granular soils considering the particle size distribution. Granular Matter 25, 35 (2023).Tsoungui, O., Vallet, D., and Charmet, J.-C.: Numerical model of crushing of grains inside two-dimensional granular materials, Powder Technology, 105(1–3), (1999), 190–198.

Wang, B., Martin, U., and Rapp, S.: Discrete element modeling of the single-particle crushing test for ballast stones, Computers and Geotechnics, 88, (2017), 61–73.

Wang, P., Karatza, Z., and Arson, C.: DEM modelling of sequential fragmentation of zeolite granules under oedometric compression based on XCT observations, *Powder Technology*, 347, (2019), 66–75.

Weibull, W.: A statistical distribution function of wide applicability, Journal of Applied Mechanics, 18(3), (1951), 293–297.

Wiacek, J., and Molenda, M.: Effect of particle size distribution on micro- and macro-mechanical response of granular packings under compression, International Journal of Solids and Structures, 51(25–26), (2014), 4189–4195.

Wu, M., Wang, J., and Zhao, B.: DEM modeling of one-dimensional compression of sands incorporating a statistical particle fragmentation scheme, Canadian Geotechnical Journal, 59(1), (2022), 144–157.

Xu, Y.: The fractal evolution of particle fragmentation under different fracture energy, Powder Technology, 323, (2018), 337–345.

Zhang, C., Chen, Y., Wang, Y., and Bai, Q.: Discrete element method simulation of granular materials considering particle breakage in geotechnical and mining engineering: A short review, Green and Smart Mining Engineering, 1(2), (2024), 190–207.

Zheng, W., and Tannant, D.D.: Grain breakage criteria for discrete element models of sand crushing under one-dimensional compression, Computers and Geotechnics, 95, (2018a), 231–239.

Zheng, W., and Tannant, D.D.: Grain breakage criteria for discrete element models of sand crushing under one-dimensional compression, Computers and Geotechnics, 95, (2018b), 231–239.

Zhou, W., Yang, L., Ma, G. et al. DEM analysis of the size effects on the behavior of crushable granular materials. Granular Matter, 18, (2016), 64.

Zhou, W., Wang, D., Ma, G., Cao, X., Hu, C., and Wu, W.: Discrete element modeling of particle breakage considering different fragment replacement modes, Powder Technology, 360, (2020), 312–323.